






Sensing Methodologies for Gait Parameters Estimation and Control

5

Maria J. Pinto-Bernal , Sergio D. Sierra M. , Marcela Múnera, and Carlos A. Cifuentes 

5.1 Introduction

Mobility is one of the essential faculties and can be defined as the ability of an individual to freely move through multiple environments and perform activities of daily living with ease [1, 2]. Following a neurological dysfunction, such as stroke, mobility may be affected and only a short period might remain to take advantage of the inherent adaptability and plasticity of the central nervous system [3]. Reestablishing adequate mobility for individuals with lower-limb impairments is often a complex challenge and frequently involves the interdisciplinary efforts of many medical, surgical, and rehabilitative specialists [4]. Thus, robotics-based training is considered a potential aid, not only for patients but also for healthcare professionals.

Although these diseases that compromise mobility are well identified and studied, just a small group of individuals can be entirely reversed by surgical or rehabilitation procedures [5]. In other words, most of the patients who suffer disorders of gait are left with consequences. In this context, it is paramount to mitigate disability and the deterioration of the quality of life of these individuals. It is necessary to develop techniques that enhance the rehabilitation processes to improve patient mobility safely and efficiently [6]. Therefore, gait analysis has been used to help therapists who wish to monitor the recovery of patients going through rehabilitation processes [7]. Within clinical settings, gait classification can be implemented as part of the control parameters for functional electrical stimulation [8, 9], estimation of the risk of older adults fall [10], the detection of

M. J. Pinto-Bernal · S. D. Sierra M. · M. Múnera · C. A. Cifuentes (✉)
Biomedical Engineering Department of the Colombian School of Engineering Julio Garavito,
Bogotá, Colombia
e-mail: maria.pinto@mail.escuelaing.edu.co; sergio.sierra@escuelaing.edu.co;
marcela.munera@escuelaing.edu.co; carlos.cifuentes@escuelaing.edu.co

abnormal gait pattern in patients with paretic limbs, and their classification based on known pathologies [11]. Besides, an atypical gait pattern can be an indicator of the progression of neurological disorders. For instance, atypical gait patterns have been proven to predict if seniors will develop dementia or cognitive decline [12].

Regarding the field of robotics, researchers have managed to program humanoid robots to use human-based gait trajectories generated via gait classification [13], as well as consistently control wearable assistive devices such as robotic prostheses [14] and orthoses [15] for the recovery of lower-limb mobility. In particular, gait phase detection methods have been used in robotic lower-limb orthoses to command force-field behaviors according to the detected gait sub-phase. Due to the recent rise in lower-limb exoskeletons as an alternative for gait rehabilitation, gait phase detection has become an increasingly important feature in controlling these devices.

This chapter aims to present strategies for the automatic identification of gait phases and their applications. To this end, firstly, it is essential to identify the importance of gait parameters to have a successful gait analysis in rehabilitation scenarios; and secondly, it is necessary to recognize the most commonly used portable devices for gait analysis with their advantages and disadvantages. The main content of this chapter is organized into five thematic sections, addressing relevant aspects regarding gait phase estimation and essential aspects covering their applications in rehabilitation settings. Section 5.2 begins with the definition of the spatiotemporal parameters that describe the gait pattern. Section 5.3 presents the most commonly used wearable gait analysis devices. Section 5.4 describes two methodologies to automatically classify and detect the gait phases for assistive and rehabilitation applications. Section 5.5 illustrates a walker-assisted gait case study, where an online methodology is presented to estimate gait parameters. Finally, Sect. 5.6 presents the conclusions and recommendations for future works in this field and the challenges of gait phases estimation in the rehabilitation context.

5.2 Spatiotemporal Gait Parameters

Spatial and temporal parameters or indicators characterize the gait cycle (presented in Chap. 1). These indicators commonly refer to the step time (seconds), stride time (seconds), step length (meters), stride length (meters), cadence (steps per minute), walking speed (meters per second), foot angle (grades), single limb support time (seconds), double limb support time (seconds), and stance-to-swing ratio. These time and distance parameters provide an index of an individual's walking patterns. It is essential to highlight that these parameters are dependent on an individual's walking speed. Therefore, it is recommended that individuals walk and their freely selected cadence during a gait analysis exam. On the other hand, although temporal gait parameters are often helpful when diagnosing pathological conditions and evaluating treatment efficacy, these parameters rarely provide sufficient insight into the origin of gait abnormalities [16].

Step length is the longitudinal distance from heel strike (HS) of one foot to contralateral HS. Step time is the elapsed time associated with the step length.

Stride length is the longitudinal distance between the occurrences of the same event (e.g., HS) with the same foot. Normal gait is symmetrical; hence, stride length is equal to twice the step length. Stride time is the elapsed time associated with the stride length. Cadence is defined as the rate at which an individual ambulates and is measured in steps per minute. The rate at which an individual ambulates at a self-selected comfortable speed is termed natural cadence. Walking speed represents the overall performance of walking. It is the rate of displacement change along the predefined direction of progression per unit time. Walking speed is also the product of step length and cadence. Foot angle is the angle between the line of progression and the foot axis. Foot angle is positive when the axis points lateral to the line of progression. Foot angle is zero when the foot axis is parallel to the line of progression. Foot angle is negative when the foot axis points medially to the line of progression. Single limb support is the elapsed time of the gait cycle during which one foot contacts the ground. Double limb support is the elapsed time of the gait cycle during which both feet are in contact with the ground. Single and double limb support may also be expressed as a percentage of the overall gait cycle. The stance-to-swing ratio is the stance interval divided by the swing interval [16–19].

5.3 Wearable Gait Analysis Devices

Gait analysis has become an essential task in clinical and rehabilitation programs, as it provides powerful insights into the individual's gait quality, the behavior of the gait pattern, and other dynamic factors [20]. Moreover, the output from a gait analysis process can offer information that is characteristic of a particular gait pathology or impairment. Thus, individualized treatments can be proposed.

Nowadays, the applications of gait analysis are divided into two main categories: clinical gait assessment and gait research purposes. Despite both seek to improve the human quality of life, clinical gait assessment (addressed in Chap. 10) has the purpose of helping individual patients directly, whereas gait research aims to improve medical diagnosis or treatment by improving the understanding of gait [21]. For instance, the gait spatiotemporal parameters are widely used in control algorithms for robotic applications and several rehabilitation programs [2, 22]. The smart walkers use gait information to provide natural and safe control strategies [2, 23]. Similarly, estimating users' gait speed is useful to implement follow-in-front controllers or intention-based strategies in smart walkers [24–26]. Furthermore, it has been demonstrated that the tracking of gait parameters during rehabilitation processes may offer an overall indicator of patients' gait health [27].

Several gait analysis methods have been used and employed in these applications according to: (1) the nature of the clinical condition, (2) the individual's skills, (3) the available facilities in the clinic or laboratory, and (4) the purpose for which the analysis is being performed [21]. In general terms, the analysis methodology strongly relies on the type of sensor used. Among the most common wearable sensors are: inertial sensors, ultrasonic sensors, laser rangefinder systems, and force sensors.

5.3.1 Inertial Sensors

Inertial sensors are gaining increasing popularity in human motion analysis, as they are commonly worn by the user, provide motion data directly, and do not require external sources or devices. Using inertial sensors can typically achieve high accuracy at moderate to high walking speeds or in self-paced walking. However, their performance noticeably degrades at lower speeds, usually the pace for individuals with walking difficulties [28, 29].

The typical inertial sensor is the Inertial Measurement Unit (IMU), a combination of three components: accelerometers, gyroscopes, and magnetometers. This device can measure gravitational force, speed, and orientation. With these parameters it is possible to make estimations of the gait phases, as well as spatiotemporal parameters [30]. The implementation of different sources of information in IMUs makes them a very robust sensor, and they often require complex fusion algorithms to get improved estimations [27].

Accelerometers are the most widely used option if an outpatient gait analysis is required; these have certain advantages such as reduced size, highly mobile, low cost, and power consumption [30]. Accelerometers are transducers used to measure linear and angular accelerations. They can be arranged in either uni- or multi-axial configurations. These devices are designed according to Newton's second law of motion and Hooke's law [31]. Displacement and velocity sensors can be used in combination with derivative circuits to measure acceleration. Direct measurement of acceleration can also be obtained with the use of compact accelerometers [31]. However, its use carries several factors such as: (1) the need for gravity compensations, (2) increased computational load in the post-processing stage, (3) the occurrence of drift error in position data, and (4) the need for system's calibration to properly locate the sensors in the required application [30].

Gyroscopes are angular velocity sensors. This velocity is a factor whose signal is not influenced by the vibrations that occur when hitting the heel, and additionally, this variable is not affected by the force of gravity. In gyroscope, the output is the obtained periodic results whose patterns are repeated during the gait cycle [30]. To get the references to the framework to these sensors as it is the orientation of the axis are commonly used the Direction Cosine Matrix (DCM) and Kalman filter [32]. Today, commercially available inertial sensors measure both linear and angular accelerations with six degrees of freedom.

Finally, magnetometers provide information related to changes in magnetic fields. By definition, these devices measure the air's magnetic flux density and detect fluctuations in Earth's magnetic field. With this information, the magnetometers offer the possibility to find the vector towards Earth's magnetic North. This is often used to improve the accuracy of the measurement system through the use of data from the magnetometer, accelerometer, and gyroscope. Commercially available inertial sensors with these three types of sensors are considered as nine degrees of freedom IMUs. They provide a more robust estimation of orientation angles (i.e.,

yaw, pitch, roll), as well as linear and angular accelerations, and employ better drift correction strategies [33].

5.3.2 Ultrasonic Sensors

An ultrasonic sensor is an electronic device that measures the distance of a target object using ultrasonic sound waves and converts the reflected sound into an electrical signal [34]. An ultrasonic sensor uses a transducer to send and receive ultrasonic pulses that relay back information about an object's proximity. These sensors, for instance, estimate the gait parameters by measuring the distance between the user's feet and the floor [27]. In general, these measure kinematic variables such as the stride length, step length, the distance separating the two feet, and the distance separating the swinging foot from the ground.

5.3.3 Laser Rangefinders (LRFs)

Laser-based systems or laser rangefinders are optical sensors that use infrared laser beams for distance measurement in two dimensions. In general, these systems consist of a transmitter of light pulses arranged on a rotation system that allows distance measurements at different angles. Most common LRFs are based on the time-of-flight principle. Under this method, the time it takes for the light beam to travel to a target and return is measured [35, 36].

The data delivered by the laser sensors can be organized as an ordered sequence of points in polar coordinates (S), as shown in Eq. 5.1, where ρ corresponds to the measured distance and θ to the angle.

$$S = [s_1, s_2, \dots, s_n], \quad s_i = (\rho, \theta). \quad (5.1)$$

In some applications it is helpful to express the points acquired by the laser in Cartesian coordinates. Considering that the plane of laser readings corresponds to the XY plane, Eq. 5.2 illustrates this conversion.

$$P = [(x_1, y_1), (x_2, y_2), \dots, (x_n, y_n)], \quad : x_i = \rho \sin(\theta), \quad \rho \cos(\theta). \quad (5.2)$$

For instance, in walker-assisted gait applications, these sensors track the user's legs position and are placed in front of the user at approximately the knee height [2, 22–24, 37]. Clustering algorithms then process the information retrieved from the LRFs to estimate the average position of each leg.

5.3.4 Foot Pressure Sensors

The ground reaction force is an external force acting on the sole during standing, walking, or running activities. In this sense, the ground reaction force has also been of interest in human motion analysis [38]. To date, numerous measurement techniques have been utilized in the study of this type of force. For instance, the ground reaction force can be measured by sensors placed on the floor [27, 39] or foot pressure sensors that measure the foot contact with the ground [40]. Other techniques include floor-mounted transducer matrices, pressure mats, instrumented shoes, force plates, insole-based pressure systems, and glass plates using the critical light reflection technique [27].

Studies utilizing floor-mounted force sensing resistors (FSR) or transducers illustrate barefoot, isolated steps, and insole systems that allow investigation of step-to-step alterations in gait. Their output requires a straightforward processing, but they do not provide any information regarding the swing phase of the gait [41]. Specifically, an FSR is a sensor whose electrical resistance changes in proportion to an applied pressure; as applied to gait phase detection, these sensors are located in shoe soles so that changes in the plantar pressure can be directly correlated to the gait phase, since each gait phase can be related to a specific pressure pattern [42–45]. Flexible pressure sensors experience changing resistances as a function of pressure. These sensors are inexpensive and have a convenient input composition [42]. Nevertheless, their use in everyday activities is not recommended as they need to be placed at optimal locations to accurately detect gait phases, thus requiring an experienced professional to determine their optimal placement [46]. Additionally, pressure insoles must be tailored for each subject's foot, which incurs higher research costs, and are continuously exposed to tear and friction, which results in a shorter lifetime [47].

Overall, although these sensors provide essential real-time information correlated to locomotion, they are low-cost and small size enabling applications in both clinical settings and home environment applications [41]. Besides, in plantar pressure studies consideration should be given to possible sources of error. These include sensor hysteresis, non-linearity, bending, humidity and temperature changes, and stress shielding secondary to sensor–tissue or sensor–insole interface mechanics [38].

5.4 Classification of Gait Phases: Exoskeletons' Case Study

The evolution of technology allows using more sophisticated tools such as pattern analysis and artificial intelligence to analyze and interpret the motion and gait analysis. These models allow accurate biomechanical analysis and precise analysis of the biomechanical effects of orthotics, prosthetics, and assistive devices. This section will show the theoretical approach, implementation methodology, and applications of two classification strategies that have been implemented in this book

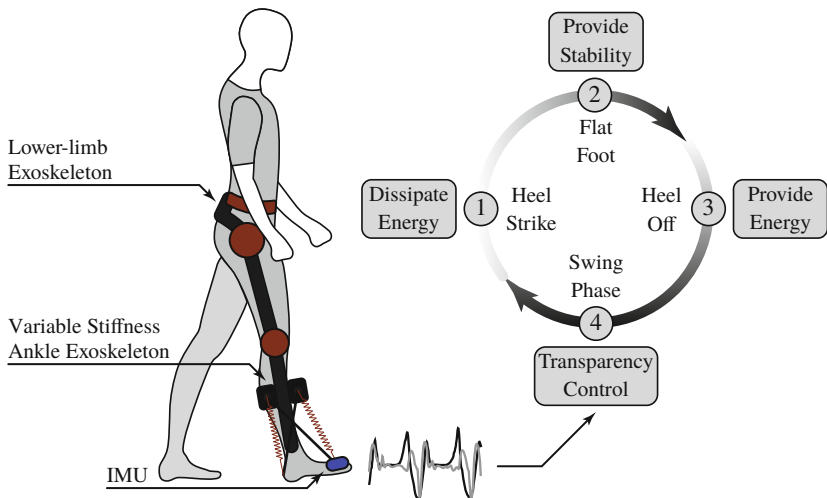


Fig. 5.1 Illustration of an assisted gait application using a lower-limb exoskeleton and a variable stiffness ankle exoskeleton. Gait phases' information is used to determine the behavior of the assistive devices

for the automatic identification of gait cycle.¹ As an illustration, Fig. 5.1 describes an example of a lower-limb exoskeleton and a variable stiffness ankle exoskeleton in a gait assisted application. The assistive devices employ the information extracted from an IMU to determine the most appropriate control strategy at each gait phase.

First, it is essential to note that several computational methods have been previously proposed for the automatic segmentation of the gait cycle, which fall into two main categories. The first category is comprised of algorithms, which divide the gait phases based on the threshold selection of either raw or processed data [44, 48]. Second, some machine learning approaches have emerged in recent years to substitute the techniques mentioned above that rely on hand-crafted feature extraction. These adaptive methods extract patterns based on Support Vector Machines (SVM) [11], Artificial Neural Network (ANN) [43, 49, 50], hybrid algorithms [51], hidden Markov model (HMM) [52–58], among others.

This chapter implements two classification strategies for the automatic identification of four gait phases, drawn from inertial data coming from a single Inertial Measurement Unit (IMU) located at the foot instep. This sensor is used as means of gait phase detection thanks to its cost-effectiveness [59] and the fact that inertial quantities present typical waveform features during a gait cycle [60]. Studies have been conducted positioning IMUs on the waist [61], thigh [62], shank [63], and foot instep [8, 64]. The IMU placed at the foot instead was because scalar classifiers have

¹The implementation of the two classification strategies and the dataset are available at: https://github.com/midasama3124/hmm_gait_phase_classifier.

shown better performance with the sensor placed at this location, even compared to other vector classifiers involving more inertial sensors placed at different locations on the lower limb [53].

Regarding the two classification strategies implemented, the first and most easily implemented strategy is a threshold-based algorithm that determines the gait phases of interest by establishing specific decision rules and thresholds, which must be met to jump from one gait phase to another. The other partitioning method may be viewed as a machine learning algorithm since it requires a training stage and a posterior testing stage [52]. Specifically, the implemented algorithm is based on a continuous HMM.

5.4.1 Threshold-Based Detection Algorithm (TB)

A Threshold-Based Detection Algorithm is based on a finite state machine (FSM), which consists of a set of states s_i and a set of transitions between pairs of states s_i, s_j . A transition is labeled condition/action: a *condition* that causes the transition to be taken and *action* that is performed when the transition is taken [65]. State machines are a method of modeling systems whose output depends on the entire history of their inputs and not just on the most recent input, compared to purely functional systems, in which the input purely determines the output. State machines have a performance determined by their history [66] and provide means to control decisions.

The developed Threshold-Based Detection (TB) Algorithm is based on the mediolateral axis rotation component of the foot accelerometer (A_y) and gyroscope (G_y) signals as input, since the lower-limb joints movement occurs mainly along the sagittal plane. Timestamps are also used as algorithm inputs, since this detection algorithm uses spatial thresholds and temporal limits. This means that each gait phase can be associated with a sequence of wave-related features without any complex processing that would result in a high computational load [67]. For more information on the TB's feature extraction process, the author recommends to read the publication associated with this chapter [68]. Figure 5.2 illustrates the feature-based conditions for the transitions between gait phases. Similar strategies based on curve characteristics could be carried out in different inertial signals drawn from different locations in the human body (i.e., waist, shank, thigh).

To be more precise, the flowchart in Fig. 5.3 summarizes the main detection features for the transition between gait phases and their extraction process. First, feature extraction from linear acceleration and angular velocity signals begins with creating a feature list, since several features must be found before any gait phase is claimed as detected. Each time a new gait phase is updated, this list is emptied. The input data ($D(i)$ in Fig. 5.3: G_y or A_y as appropriate) are updated at a sampling rate of 100 Hz, which matches the inertial sensor sampling rate. Each feature should meet certain conditions to be included in the list. These conditions are evaluated sequentially as follows:

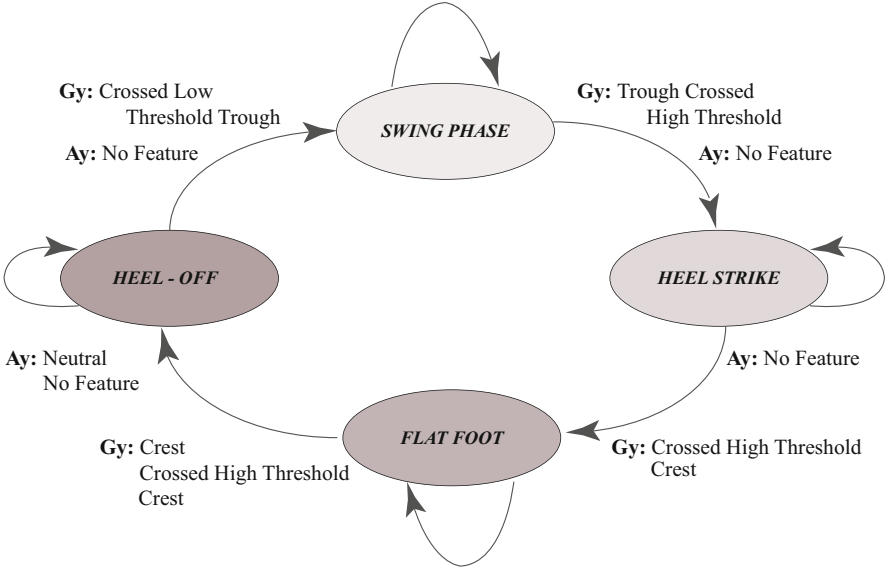


Fig. 5.2 State machine of the threshold-based algorithm. The transition conditions are based on features found in the angular velocity (G_y) and linear acceleration (A_y) signals

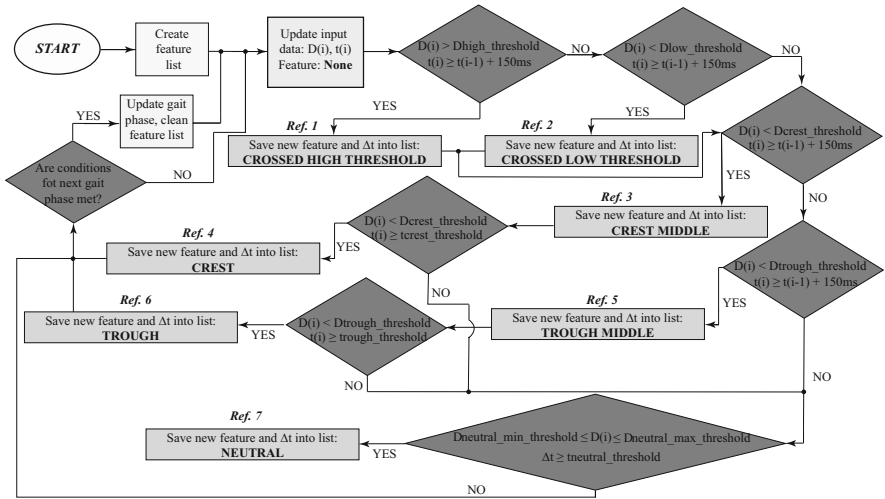


Fig. 5.3 Flowchart of feature extraction of the threshold-based algorithm from inertial motion data. This chart shows how a feature list is updated based on the fulfillment of certain conditions. The occurrence of each feature and their corresponding conditions are sequentially assessed in the following manner: crossed high threshold (Ref. 1), crossed low threshold (Ref. 2), Crest Middle (Ref. 3), crest (Ref. 4), Trough Middle (Ref. 5), Trough (Ref. 6), and neutral (Ref. 7). When a new gait phase is detected, the feature list is emptied for further searches. Adapted from [68]

- **Crossed High Threshold (Ref. 1 in Fig. 5.3):** Current data ($D(i)$) must be above a pre-established threshold ($D_{\text{high_threshold}}$) and at least 150 ms should have elapsed since the last saved feature. The time difference between features (Δt) and the spotted feature is saved into the feature list.
- **Crossed Low Threshold (Ref. 2 in Fig. 5.3):** Current data ($D(i)$) must be below a pre-specified threshold ($D_{\text{low_threshold}}$) and at least 150 ms should have elapsed since the last saved feature. Also Δt is saved into the feature list.
- **Crest Middle (Ref. 3 in Fig. 5.3):** Current data ($D(i)$) must be above a pre-established threshold ($D_{\text{crest_threshold}}$), and at least 150 ms should have elapsed since the last saved feature. Also, Δt is saved into the feature list.
- **Crest (Ref. 4 in Fig. 5.3):** This feature is only assessed if *Crest Middle* has been saved into the list. Hence, the current data ($D(i)$) must have crossed the already exceeded pre-specified threshold ($D_{\text{crest_threshold}}$), and a certain amount of time ($t_{\text{crest_threshold}}$), which differs between acquired signals (A_y , G_y), should have elapsed since the last saved feature. Therefore, a crest may be reported. Also, Δt is saved into the feature list.
- **Trough Middle (Ref. 5 in Fig. 5.3):** Current data ($D(i)$) must be below a pre-specified threshold ($D_{\text{trough_threshold}}$) and at least 150 ms should have elapsed since the last saved feature. Also, Δt is saved into the feature list.
- **Trough (Ref. 6 in Fig. 5.3):** This feature is only assessed if *Trough Middle* has been saved into the list. Hence, the current data ($D(i)$) should again be above the already crossed pre-specified threshold ($D_{\text{trough_threshold}}$), and a certain amount of time ($t_{\text{trough_threshold}}$), which differs between acquired signals (A_y , G_y), should have elapsed since the last saved feature. Therefore, a crest may be reported. Also, Δt is saved into the feature list.
- **Neutral (Ref. 7 in Fig. 5.3):** A neutral region is only reported as long as the current data ($D(i)$) remains within the range between $D_{\text{neutral_min_threshold}}$ and $D_{\text{neutral_max_threshold}}$, and if a certain amount of time ($t_{\text{neutral_threshold}}$), which differs between acquired signals (A_y , G_y), has elapsed since the last saved feature. Also, Δt is saved into the feature list.

The selection of correct threshold values used in this classifier was carried out as reported in *Kotiadis et al.* [69], whose research validated all possible thresholds within a range, and whose limits were determined visually from the signals captured in a preliminary analysis. After checking each condition included in the feature extraction process (as evidenced above), the feature list is reviewed to determine if a new gait phase has been found. The following is a summary of the feature-based rules governing the various transitions between gait phases.

- **Heel Strike (HS) → Flat Foot (FF):** To detect the FF onset, the current angular velocity signal must have exhibited a crest, while the linear acceleration data must be right in the middle of a trough, after entering the crest corresponding to the HS in the feature list (see Fig. 5.4).

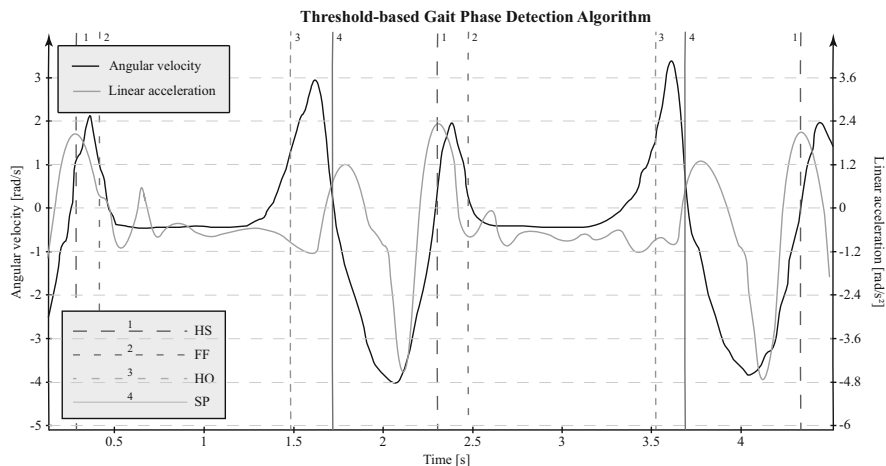


Fig. 5.4 Threshold-based gait phase detection using an inertial detection system over two gait cycles. Feature-based decisions are made to identify the onset of each gait phase: heel strike (first dashed line), Flat Foot (second dashed line), heel off (third dashed line), and swing phase (fourth complete line). Adapted from [68]

- **Flat Foot (FF) → Heel Off (HO):** To detect the HO onset, the current angular velocity signal has a neutral region, since linear acceleration data also must remain within a neutral region, followed by a high cross threshold (see Fig. 5.4).
- **Heel Off (HO) → Swing Phase (SP):** To detect the SP onset, the current angular velocity signal must have shown a crest, while the linear acceleration data must have crossed a predefined threshold (see Fig. 5.4).
- **Swing Phase (SP) → Heel Strike (HS):** To detect the HS onset, the current velocity signal should have shown a trough and a crossed high threshold, while the linear acceleration data should be in the middle of a crest, and after another crest, a trough and a crossed high threshold have been sequentially entered in the feature list (see Fig. 5.4).

5.4.2 Classification Using a Hidden Markov Model (HMM)

A Markov process is a stochastic extension of a finite state automaton. It provides a way to model the dependencies of current information with previous information. In a Markov process, state transitions are probabilistic and there is in contrast to a finite state automaton no input to the system: besides, it is composed of states, transitions, scheme between states, and emission of outputs (discrete or continuous) [70, 71]. The following can be achieved with Markov's models: Learning sequential data statistics, making predictions or estimates, and recognizing patterns.

An HMM is a double stochastic process in which the existence of a set of discrete states is assumed for a given system. The first stochastic process describes how the system may jump from one state to another (transition probability), under the hypothesis that the next state depends only on the state at present (Markov property). It means that this process has N underlying discrete states that are not observable, i.e., its state sequence is hidden to the observer who only has access to the emissions of each state [72]. In this case, this first stochastic process refers to the gait cycle, which was divided into four phases (this division is the most used as illustrated in Chap. 1). On the other hand, the second stochastic process yields the statistical description governing the emissions of each observed variable (emission probability). It means that the second embedded stochastic process describes the emissions from Y observations, i.e., either the sensor readout or feature vectors extracted from them (in this case they were the signals given by the IMU sensor), in terms of discrete probabilities or Probability Density Functions [54]. HMM is a statistical model widely used to estimate a sequence of hidden states in a time series [52], which for the case of gait phase detection corresponds to the gait events ($N = 4$), i.e., Flat Foot, Toe Off, Swing, and heel strike.

The HMM can be expressed as a function, as presented in Eq. 5.3 as a set λ characterized of three parameters A , B , and π .

$$\lambda = (A, B, \pi), \quad (5.3)$$

which includes the probability distribution matrix of state transition A , the probability distribution matrix of observation symbols B , and the initial state distribution vector π .

The typical gait pattern repeats itself indefinitely with a known sequence of gait events, which in terms of probability means that it can either remain in the current state or eventually transition to the consecutive state. This behavior has recently been modeled using a left–right model [53, 54], whose main feature is to limit transitions to consecutive states of the Markov chain. Since transitions represent a narrow fraction of the gait cycle, their associated probabilities assume lower values than those related to permanence in the same state. Thus, diagonal elements assume a higher value than the others. Therefore, the transition matrix A may be implemented as shown in Eq. 5.4 [53].

$$A = \{a_{ij}\} = \begin{bmatrix} 0.9 & 0.1 & 0 & 0 \\ 0 & 0.9 & 0.1 & 0 \\ 0 & 0 & 0.9 & 0.1 \\ 0.1 & 0 & 0 & 0.9 \end{bmatrix}, \quad (5.4)$$

where a_{ij} denotes the transition probability from state S_i to state S_j . The possible transitions among gait phases are reported in Fig. 5.5. The state S_I was paired to the gait phase delimited by swing phase and heel strike events. Further pairings were:

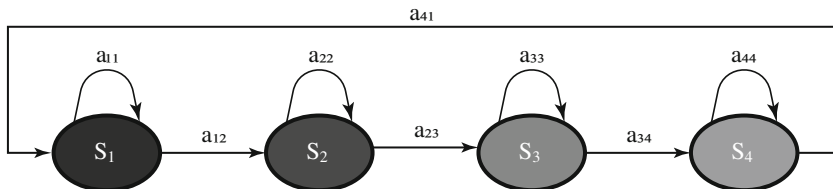


Fig. 5.5 Possible transitions (a_{ij}) among four states (S_i) of a continuous HMM according to a left–right model. Each model state is paired to a gait phase, whose borders are identified by corresponding gait events and whose emissions are modeled using a Gaussian Mixture Model with three components: a_{ij} denotes the transition probability from state S_i to state S_j

S2: Heel Strike—Stance Phase; S3: Stance Phase—Toe Off; S4: Toe Off—Swing of the next stride.

Because the initial state t_0 of the model is unknown, an initial state distribution vector π allocates the same probability to all states (see Eq. 5.5), i.e., each state has the same probability of being the first in a chosen state sequence.

$$\pi = \{t_0\}_{Q \times 1} = \begin{pmatrix} \frac{1}{N} \\ \frac{1}{N} \\ \frac{1}{N} \\ \frac{1}{N} \end{pmatrix} = \begin{pmatrix} 0.25 \\ 0.25 \\ 0.25 \\ 0.25 \end{pmatrix}. \tag{5.5}$$

Finally, a Bivariate Gaussian Mixture Model with three components was utilized to describe the emissions from each state. These emissions allude to feature vectors that include the angular velocity measured at any sampling time, and its time derivative computed employing a first-order finite difference approximation, i.e., the angular acceleration [55]. This particular stochastic model yields the best trade-off between complexity and accuracy for gyroscope signals [54, 62].

It is essential to highlight that to develop an HMM is necessary to consider the three problems learning/interference and three algorithms to help to solve these problems: the Baum–Welch (BW) algorithm computes the Maximum Likelihood (ML) estimates of model parameters; the Viterbi algorithm estimates the most likely sequence of hidden states; the forward–backward algorithm [72].

The continuous HMM development involves two main procedures: a training phase and a test phase. The first stage concerns the adjustment of model parameters λ to optimally fit them to an observed training dataset [72]. In the present classifier, the Baum–Welch algorithm, which is the most common solution to this problem, is implemented. This training procedure starts with a set of initial parameters (*first-phase training* in Fig. 5.6), based on which it extracts probabilistically weighted state sequences. The initial model is repeatedly updated with these new transition and emission probabilities until a desired level of convergence is reached [62].

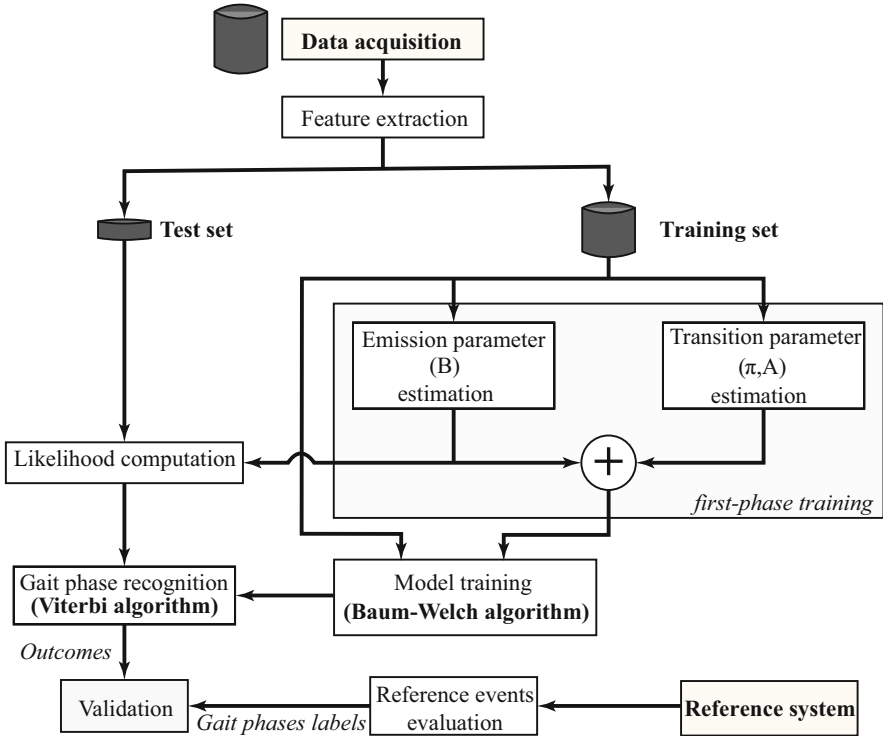


Fig. 5.6 Flowchart that illustrates the validation methodology of HMM. A model is trained to employ the Baum–Welch algorithm after applying feature extraction to the acquired dataset. The optimal state sequence is then computed through the Viterbi algorithm by using feature vectors from the test dataset, and the performance evaluation is conducted concerning gait phase labels drawn from the reference system. Adapted from [68]

Afterward, the testing stage allows the classification of features based on the trained model reached in the training phase, i.e., the search for the optimal state sequence is carried out. The Viterbi algorithm uses a common optimality criterion to find the most likely/probable state sequence [72]. Despite its computational efficiency, this algorithm is not suitable for real-time application, since the indicators it uses are computed based on a whole observation dataset. Therefore, the validation of the classifier outputs is compared offline concerning an FSR-based reference system that provides the actual gait phase labels. The reference system should be matched with each subject's shoe size and equipped with four force-sensitive resistors (FSRs) on the foot sole. The first sensor is located at the hallux (toe), two more sensors are located at the first and fifth metatarsophalangeal articulation, and one more is located at the heel.

5.5 Estimation of Gait Parameters: Smart Walkers' Case Study

As previously described, gait characterization is often accomplished by calculating spatiotemporal parameters, such as speed, cadence, stride length, step length, among others. Some of these features are referred to as the general gait parameters (GGPs) and have been widely used as standard indicators for gait assessment [73]. Among the GGPs, three spatial and temporal parameters are found: (1) the stride cadence (SC), (2) the stride length (STL), which is composed of two step lengths (SPL); and (3) the gait speed (GS) [73, 74].

To estimate the GGPs, many studies have proposed and assessed sensing technologies comprising wearable and non-wearable sensors [37]. However, most of them have been developed within laboratory conditions, with non-wearable constraints, and do not allow online estimations [75]. Therefore, an accurate online estimation of these parameters with ambulatory technologies for practical scenarios is described in the following sections [37].

5.5.1 Gait Data Acquisition

The first step in estimating gait parameters is acquiring data from the patient or user of an assistive device. For this description, a walker-assisted gait application was proposed, in which a laser rangefinder (LRF) sensor is used to detect and track the user's legs relative position. Figure 5.7a shows an example of the LRF's location and orientation in a passive rollator application.

In ambulatory applications employing LRF sensors and mobile assistive devices, such as smart walkers, it is essential to place the sensor at an appropriate height guaranteeing that the laser's field of view is not occluded and the user's legs are always visible. Given the variability in gait patterns from one individual to another, a proper recommendation on the LRFs location is to place them approximately at the user's knees height [37]. This location provides a clear field of view, even in self occlusions during walking (i.e., the legs are too close or one in front of the other). Figure 5.7b and c illustrates examples of LRF's readings during walker-assisted gait.

In addition to the above, to avoid noisy readings with objects not related to users' legs, the measurement area is often constrained to a narrow polygon. Notably, the LRF's field of view is constrained between 45° and 135° and between 1 m and 1.5 m.

5.5.2 Clustering of Legs' Data

Once data are obtained from the LRF sensor, it is essential to label the laser readings, to identify which leg they are from. To this end, different machine learning algorithms are often used for classification purposes. One of the most common techniques relies on an unsupervised learning classifier that returns clusters of laser

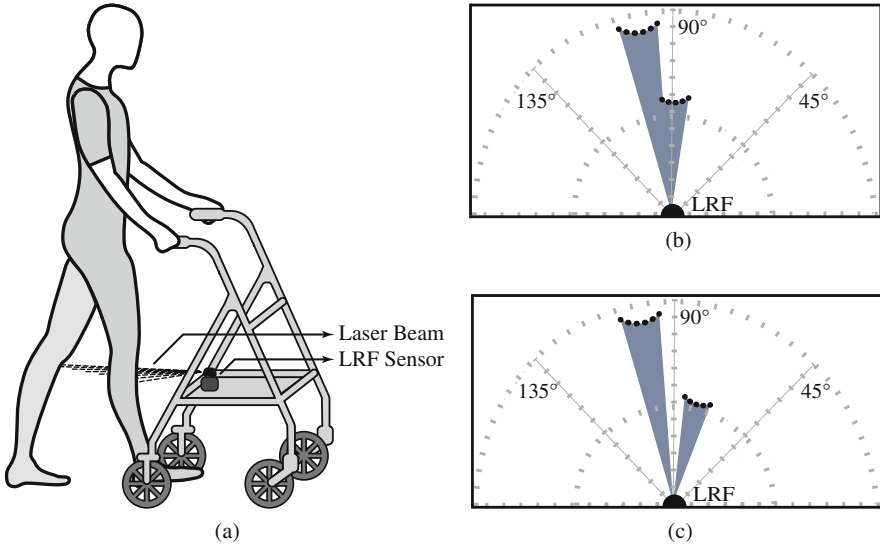


Fig. 5.7 (a) Illustration of an assisted gait application with a passive rollator, equipped with a laser rangefinder (LRF) to detect and track the user's legs. (b) Example of LRF scan where one leg is covering part of the other leg. (c) Example of LRF scan where legs are enough separated

points [24, 37]. For instance, density-based spatial clustering of applications with noise (DBSCAN) is one of the most used data clustering algorithms that, in this case, allows the classification of laser points either as legs or as noise [24].

These clustering algorithms require two parameters to be executed. The first one refers to the minimum distance to group two consecutive points. The second one defines the minimum number of grouped points to save a cluster [24]. After that, the position of each leg and relative distance to the walker can be defined by calculating the center of each cluster and the mean distance between them [24].

5.5.3 Legs' Distance Difference (LDD) Signal

During gait, the human trunk exhibits oscillatory behavior, and so does the movement of the legs. In particular, the distance between the legs is characterized by a sinusoidal behavior. Therefore, to estimate the GGPs, this signal can be used. The frequency and amplitude of the principal component of the signal obtained from a distance between each leg correspond to the stride cadence (SC) and the step length (SPL), respectively [2]. Moreover, it is possible to estimate the gait speed (GS), by multiplying the SC and the SPL [76]. Using the LRF readings, the LDD signal can be calculated as described in Eq. 5.6.

$$LDD = d_R * \sin(\theta_R) - d_L * \sin(\theta_L), \quad (5.6)$$

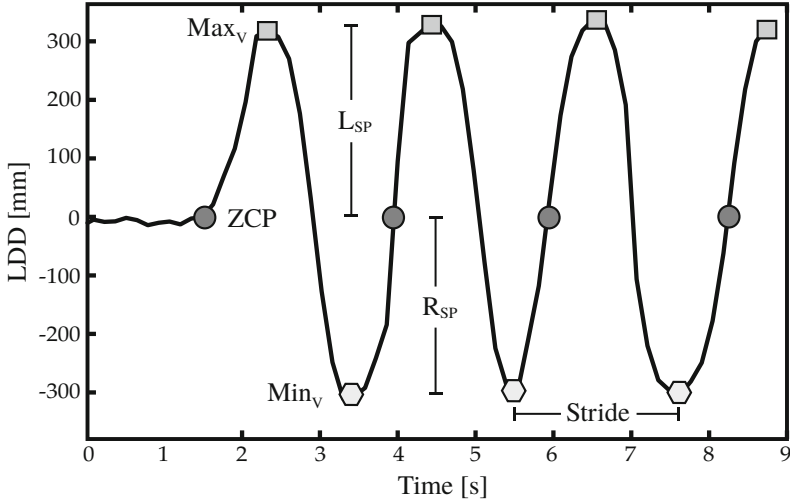


Fig. 5.8 Illustration of the legs' distance difference (LDD) signal, obtained from the readings of the LRF sensor

where d_R and d_L are the distances to the right and left legs, respectively; θ_R and θ_L are the angles of the right and left legs. Each cycle of the LDD signal illustrates the behavior of a stride cycle composed of two steps. The right step (R_{SP}) can be seen as a decrease in the LDD signal and the left step (L_{SP}) can be seen as an increase in the LDD signal. Moreover, the length of each step can be calculated by the maximum value (Max_{LDD}) and minimum values (Min_{LDD}) of each cycle. Thus, the stride length (STL) can be estimated as the sum of both step lengths.

To extract every cycle of the LDD signal, the zero crossings with positive slopes (ZCP) provide the starting and ending points of each stride. With this information, the SC can be calculated as the inverted value of the period of each cycle [2]. Figure 5.8 illustrates the LDD signal, describing the left and right steps (R_{SP} , L_{SP}), the zero crossings with positive slopes (ZCP), and the maximum values (Max_{LDD}) and the minimum values (Min_{LDD}) of each cycle.

5.5.4 Adaptive Filters for LDD Processing

A simple approach to estimate the GGPs would use the Max_{LDD} , Min_{LDD} , and ZCP values to calculate the frequency and amplitude of the LDD signal. However, this method might be affected by sudden objects sensed by the LRF or noisy readings. Therefore, a robust methodology based on two adaptive filters has been proposed to estimate the GGPs [37]. In particular, the Weighted Frequency Fourier Linear Combiner (WFLC) and the Fourier Linear Combiner (FLC) are filters that allow a smooth online estimation of the frequency and amplitude of the principal Fourier component of the LDD signal [37]. In this sense, the WFLC takes the LDD

signal as input and estimates the stride cadence, while the FLC takes the LDD signal and the stride cadence to estimate the step length. According to the literature evidence, these filters have proven to be valuable and efficient in several real-time applications [2, 22, 77, 78].

5.5.4.1 Weighted Frequency Fourier Linear Combiner (WFLC)

In general terms, the WFLC filter is a powerful tool capable of calculating the frequency, amplitude, and phase of the Fourier components from a real-time signal [79]. The WFLC filter uses the least mean square algorithm to reduce the error between the actual signal and the estimated signal conformed by the Fourier components. The process of the WFLC filter can be described as follows in Eqs. 5.7, 5.8, 5.9, and 5.10 [37]:

$$x_{rk} = \begin{cases} \sin(r \sum_{t=1}^M \omega_{0t}), & 1 \leq r \leq M \\ \cos(r \sum_{t=1}^M \omega_{0t}), & M + 1 \leq r \leq 2M \end{cases} \quad (5.7)$$

$$\varepsilon_k = S_k - \mu_b - \mathbf{W}_k^T \mathbf{X}_k \quad (5.8)$$

$$\omega_{0k+1} = \omega_{0k} + 2\mu_0 \varepsilon_k \sum_{r=1}^M r (W_{rk} X_{m+rk} - W_{m+rk} X_{rk}) \quad (5.9)$$

$$\mathbf{W}_{k+1} = 2\mu_1 \varepsilon_k \mathbf{X}_k + \mathbf{W}_k. \quad (5.10)$$

Equation 5.7 describes the estimation of the Fourier components with an initial guess of the frequency ω_{0t} . Equation 5.8 illustrates the calculation of the error between the input signal (S_k) and the estimated signal conformed by the Fourier components (\mathbf{W}_k represents a matrix containing the weights of each Fourier component, and \mathbf{X}_k represents a matrix with each Fourier component value). Equations 5.9 and 5.10 show the implementation of the least mean square algorithm to update the frequency (ω_{0k+1}) and the amplitudes (\mathbf{W}_{k+1}) [37].

It is worth mentioning that the WFLC formulation requires four parameters to be set or tuned: (1) M , the number of required harmonics to estimate the input signal (set to 1); (2) μ_0 , the gain used to adapt the frequency estimation (set to 0.14); (3) μ_1 , the gain used to adapt the amplitude estimation (set to 0.4); and (4) μ_b , the gain used to compensate low-frequency errors (set to 0) [80]. A normalization value (NV) of 1000 was used to set the signal between -1 and 1 [37, 79].

As an illustration of a walker-assisted gait application, Fig. 5.9 shows a comparison between the stride cadence obtained by the WFLC (SC_{WFLC}) and the estimated

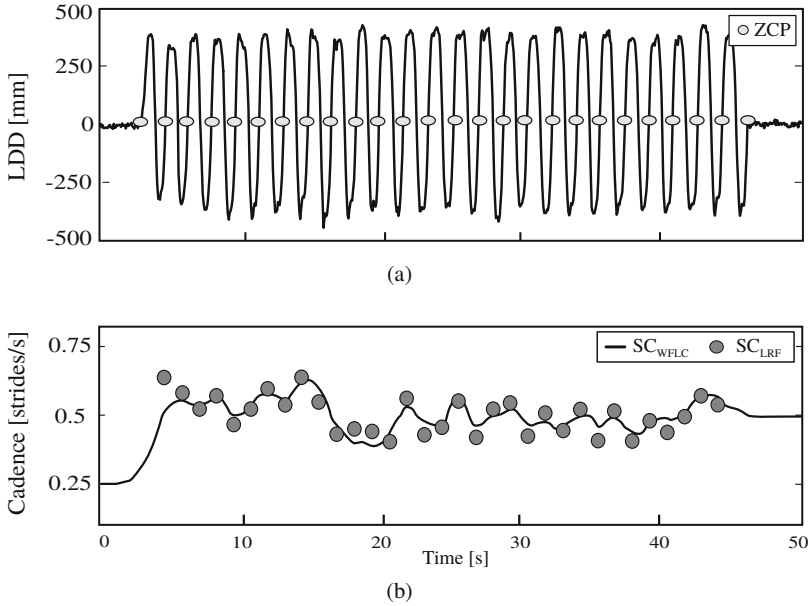


Fig. 5.9 Example of the Weighted Fourier Linear Combiner (WFLC) behavior in a walker-assisted gait application at a speed of 1.8 km/h. (a) Illustration of the legs' distance difference signal (LDD) and the zero crossings with positive values (ZCP). Illustration of the stride cadence obtained with the WFLC filter and the ZCP values

one with the period of each cycle (SC_{LRF}). The WFLC filter generates the SC_{WFLC} by taking the LDD signal as input, whereas the SC_{LRF} is obtained with the ZCP values of the LDD signal. The WFLC returns the SC value as soon as a sample of the input signal appears. For this example, the Hokuyo URG-04LX-UG01 was used, which works at a sample rate of 10 Hz. In this sense, the SC_{WFLC} was updated every 0.1 s. Similarly, the SC_{LRF} was only updated every time a new ZCP was detected [37]. Figure 5.9a shows the LDD signal and ZCP values obtained with the LRF at a walking speed of 1.8 km/h. Moreover, Fig. 5.9b shows the cadence obtained with the WFLC and with the ZCP values.

5.5.4.2 Fourier Linear Combiner (FLC)

The FLC is an adaptive algorithm used to achieve a continuous estimation of quasi-periodical signals based on the M harmonics dynamic Fourier mode [81]. Using a frequency and number of harmonics as inputs, the FLC can estimate the amplitudes and phases of the Fourier components. In this application, the algorithm requires the frequency (ω_0) of the signal produced by the WFLC as an input parameter [37].

Even though the WFLC also estimates the Fourier components' amplitudes, these calculations can be affected by the frequency estimation. Therefore, it is better to estimate such amplitudes employing the FLC [2]. The formulation of this filter uses

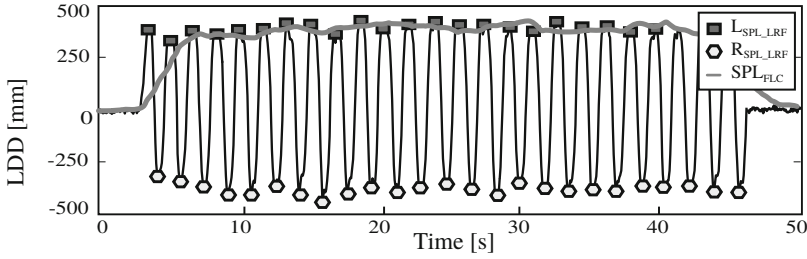


Fig. 5.10 Example of the Fourier Linear Combiner (FLC) behavior in a walker-assisted gait application at a speed of 1.8 km/h. The step length (SPL_{FLC} , in black) is estimated from the legs' distance difference (LDD, in gray) signal. The left and right step lengths (L_{SPL_LRF} , R_{SPL_LRF}) are also shown for comparison purposes

two parameters: (1) M , the number of harmonics to estimate the input signal (set to 1) and (2) μ , the gain used to calculate the harmonics weights (set to 0.2). Similar to WFLC, the FLC also employs the least mean square recursion to update the estimations of the amplitude and phase. This algorithm is described as follows by Eqs. 5.11, 5.12, and 5.13 [37, 81].

$$x_{rk} = \begin{cases} \sin(r\omega_0k), & 1 \leq r \leq M \\ \cos((r - M)\omega_0k), & M + 1 \leq r \leq 2M \end{cases} \quad (5.11)$$

$$\varepsilon_k = Y_k - \mathbf{W}_k^T \mathbf{X}_k \quad (5.12)$$

$$\mathbf{W}_{k+1} = 2\mu\varepsilon_k \mathbf{X}_k + \mathbf{W}_k, \quad (5.13)$$

where Y_k is the input signal, \mathbf{W} and \mathbf{X} matrices are the weights and values of the Fourier components, and ε_k is the error between the input signal and the estimated one. The FLC also requires a normalization value for setting the input values, between -1 and 1 .

As previously described, with the amplitude estimated by the FLC, the step length values can be directly computed. Following the walker-assisted gait example used for the WFLC illustration, the step length was estimated using the FLC output (SPL_{FLC}). This estimation was compared with the left step length, (L_{SPL_LRF}) and the right step length (R_{SPL_LRF}) calculated with maximum value MAX_{LDD} and minimum value Min_{LDD} of each LDD signal's cycle. Figure 5.10 illustrates these estimations.

Finally, to obtain the gait speed (GS), the stride cadence (SC) and the step length (SPL) calculated with the WFLC and FLC are multiplied as shown in Eq. 5.14 [37].

Table 5.1 Comparison of estimation errors between multiple technologies reported in the literature and the online methodology using an LRF sensor and adaptive filters

	Ultrasonic	Accelerometers	Gyroscopes	IMUs	LRF
SC	4.1 [82] %	5% [59]	10% [39]	2.3% [83]	4.9%
SPL	–	7% [59]	–	7% [83]	4.1%

$$GS = 2(SC)(SPL). \quad (5.14)$$

This process is not a heavy computational task and it is also carried out with every scan reading. Thus all the GGPs are computed every 0.1 s for this scenario.

5.5.5 Online Estimation

This methodology can be easily extended to an online version with simple mathematical correction. In *Aguirre et al.*, the authors found that the stride cadence does not exhibit significant differences at any speed, when comparing this methodology with an automated motion tracking system (e.g., VICON, BTS) [37]. In contrast, the step length presented significant differences with a reference system (i.e., motion tracking system). To fix this discrepancy, the authors proposed a linear model was to adjust the step length measurements.

In particular, the error between the estimation of this methodology and a reference system increases when the stride cadence does. By comparing the GGPs measurement in ten volunteers at four different speeds, the authors found the linear model presented in Eq. 5.15.

$$K = 0.157(SC) + 1.069. \quad (5.15)$$

In this way, the online estimation process goes as follows: (1) the user's legs are detected and tracked with the LRF sensor, (2) a clustering algorithm is applied to estimate the distance difference between legs (i.e., the LDD signal), (3) the WFLC estimates the frequency of the LDD's Fourier principal component (i.e., the SC), (4) the FLC uses the SC as input to estimate the amplitude of the LDD's Fourier principal component (i.e., the SPL), (5) the linear model described in Eq. 5.15 is used to adjust the SPL, and finally (vi) the GS is obtained using Eq. 5.14.

As reported by the authors in *Aguirre et al.* [37], this methodology was able to attain very accurate estimations compared to the literature evidence. In particular, Table 5.1 summarizes the estimation errors of real-time technologies, and the estimation errors for the SC and the SPL, using this online methodology. Considering that LRF sensors are commonly used to control robotic devices, such as smart walkers, rather than to do gait assessment, an average error of 5% can be considered as a good accuracy [2, 23, 24, 37].

According to the collected data in [37], it was reported that a scanning frequency of at least ten times the stride cadence is required to ensure the proper performance

of the WFLC and FLC filters. This means that to obtain an online GGP's estimation system at walking speeds of 5 km/h to 6 km/h (i.e., the average speed of healthy individuals), an LRF working at frequencies from 10 Hz to 20 Hz would be required.

5.6 Conclusions

The analysis of gait patterns, indicators, and phases is a fundamental aspect when evaluating assistive technologies, both conventional and robotic. In general, gait evaluation techniques allow to: (1) track and report a patient's rehabilitation progress, (2) detect anomalies in the gait pattern, and (3) obtain reference inputs for high-level controllers in mobile and wearable robotic devices.

According to evidence in the literature, multiple sensing technologies have been developed to acquire information about an individual's gait. In this sense, this chapter presented a brief description of the most relevant spatial and temporal indicators used to characterize human gait, and some wearable sensors that allow their acquisition for rehabilitation and daily living scenarios. Finally, multiple methodologies that allow the concise description of the different gait characteristics, including their classification by phases and calculation of the most relevant indicators, were also presented.

References

1. D.A. Winter, *Biomechanics and Motor Control of Human Movement*, 4th edn. (Wiley, Hoboken, NJ, 2009)
2. C.A. Cifuentes, A. Frizera, *Human-Robot Interaction Strategies for Walker-Assisted Locomotion*. Springer Tracts in Advanced Robotics, vol. 115 (Springer International Publishing, Cham, 2016)
3. D.M. Wolpert, J. Diedrichsen, J.R. Flanagan, Principles of sensorimotor learning. *Nat. Rev. Neurosci.* **12**, 739–751 (2011)
4. P.F. Pasquina, C.G. Emba, M. Corcoran, *Lower Limb Disability: Present Military and Civilian Needs* (Springer, New York, NY, 2017)
5. Z.O. Abu-Faraj, G.F. Harris, P.A. Smith, S. Hassani, Human gait and Clinical Movement Analysis, in *Wiley Encyclopedia of Electrical and Electronics Engineering* (Wiley, Hoboken, NJ, 2015), pp. 1–34
6. C. Vaughan, B. Davis, J. O'Connor, The three-dimensional and cyclic nature of gait, in *Dynamics of Human Gait*, vol. 168 (1999), pp. 16–17
7. J.F. Veneman, R. Kruidhof, E.E. Hekman, R. Ekkelenkamp, E.H. Van Asseldonk, H. Van Der Kooij, Design and evaluation of the lopes exoskeleton robot for interactive gait rehabilitation. *IEEE Trans. Neural Syst. Rehabil. Eng.* **15**(3), 379–386 (2007)
8. J. Rueterbories, E.G. Spaich, O.K. Andersen, Gait event detection for use in FES rehabilitation by radial and tangential foot accelerations. *Med. Eng. Phys.* **36**, 502–508 (2014)
9. J.-U. Chu, K.-I. Song, S. Han, S.H. Lee, J.Y. Kang, D. Hwang, J.-K.F. Suh, K. Choi, I. Youn, Gait phase detection from sciatic nerve recordings in functional electrical stimulation systems for foot drop correction. *Physiol. Measure.* **34**, 541–565 (2013)
10. W.-C. Wen-Chang Cheng, D.-M. Ding-Mao Jhan, Triaxial accelerometer based fall detection method using a self-constructing cascade-AdaBoost-SVM classifier. *IEEE J. Biomed. Health Inf.* **17**, 411–419 (2013)

11. A. Mannini, D. Trojaniello, A. Cereatti, A. Sabatini, A machine learning framework for gait classification using inertial sensors: application to elderly, post-stroke and Huntington's disease patients. *Sensors* **16**, 134 (2016)
12. O. Beauchet, G. Allali, G. Berrut, C. Hommet, V. Dubost, F. Assal, Gait analysis in demented subjects: interests and perspectives. *Neuropsychiatr. Dis. Treat.* **4**, 155–160 (2008)
13. J. Figueiredo, C. Ferreira, C.P. Santos, J.C. Moreno, L.P. Reis, Real-time gait events detection during walking of biped model and humanoid robot through adaptive thresholds, in *2016 International Conference on Autonomous Robot Systems and Competitions (ICARSC)*, May 2016 (IEEE, New York, 2016), pp. 66–71
14. H.T.T. Vu, F. Gomez, P. Cherule, D. Lefeber, A. Nowé, B. Vanderborght, ED-FNN: a new deep learning algorithm to detect percentage of the gait cycle for powered prostheses. *Sensors (Basel, Switzerland)* **18**(7), 2389 (2018)
15. S. Murray, M. Goldfarb, Towards the use of a lower limb exoskeleton for locomotion assistance in individuals with neuromuscular locomotor deficits, in *2012 Annual International Conference of the IEEE Engineering in Medicine and Biology Society*, vol. 2012 (IEEE, New York, 2012), pp. 1912–1915
16. R.B. Davis, Reflections on clinical gait analysis. *J. Electromyogr. Kinesiol.* **7**(4), 251–257 (1997)
17. M.W. Whittle, Clinical gait analysis: a review. *Human Movement Sci.* **15**(3), 369–387 (1996)
18. D. Sutherland, R. Olshen, E. Biden, *The Development of Mature Walking* (Cambridge University Press, Cambridge, 1988)
19. J. Perry, J.M. Burnfield, *Gait Analysis. Normal and Pathological Function*, 2nd edn. (Slack, Thorofare, 2010)
20. J. Marín, T. Blanco, J.J. Marín, A. Moreno, E. Martitegui, J.C. Aragüés, Integrating a gait analysis test in hospital rehabilitation: a service design approach. *PLoS One* **14**, e0224409 (2019)
21. M.W. Whittle, *Gait Analysis: An Introduction* (Butterworth-Heinemann, Oxford, 2014)
22. J. Casas, N. Cespedes, M. Múnera, C.A. Cifuentes, Human–robot interaction for rehabilitation scenarios, in *Control Systems Design of Bio-Robotics and Bio-mechatronics with Advanced Applications* (Elsevier, 2020), pp. 1–31
23. S. Sierra, M. Garzon, M. Munera, C.A. Cifuentes, Human–Robot–Environment interaction interface for smart walker assisted gait: AGoRA walker. *Sensors* **19**(13), 2897 (2019)
24. W.M. Scheidegger, R.C. de Mello, S.D. Sierra M., M.F. Jimenez, M.C. Munera, C.A. Cifuentes, A. Frizera-Neto, A novel multimodal cognitive interaction for walker-assisted rehabilitation therapies, in *2019 IEEE 16th International Conference on Rehabilitation Robotics (ICORR)*, June (IEEE, New York, 2019), pp. 905–910
25. J. Ballesteros, C. Urdiales, A.B. Martinez, M. Tirado, Online estimation of rollator user condition using spatiotemporal gait parameters, in *International Conference on Intelligent Robots and Systems (IROS)* (2016), pp. 3180–3185
26. C.A. Cifuentes, C. Rodriguez, A. Frizera, T. Bastos, Sensor fusion to control a robotic walker based on upper-limbs reaction forces and gait kinematics, in *5th IEEE RAS & EMBS International Conference on Biomedical Robotics and Biomechatronics* (2014), pp. 1098–1103
27. A. Muro-de-la Herran, B. Garcia-Zapirain, A. Mendez-Zorrilla, Gait analysis methods: an overview of wearable and non-wearable systems, highlighting clinical applications. *Sensors* **14**, 3362–3394 (2014)
28. A. Mannini, A.M. Sabatini, Gait phase detection and discrimination between walking–jogging activities using hidden Markov models applied to foot motion data from a gyroscope. *Gait Posture* **36**(4), 657–661 (2012)
29. S. Crea, S.M.M. De Rossi, M. Donati, P. Reberšek, D. Novak, N. Vitiello, T. Lenzi, J. Podobnik, M. Muniñ, M.C. Carrozza, Development of gait segmentation methods for wearable foot pressure sensors, in *2012 Annual International Conference of the IEEE Engineering in Medicine and Biology Society* (IEEE, New York, 2012), pp. 5018–5021
30. J. Taborri, E. Palermo, S. Rossi, P. Cappa, Gait partitioning methods: a systematic review. *Sensors* **16**(1), 66 (2016)

31. J.D. Bronzino, *Biomedical Engineering Handbook 2*, vol. 2 (Springer Science & Business Media, Berlin/Heidelberg, 2000)
32. G. Welch, G. Bishop, Others, An introduction to the Kalman filter. Technical report, University of North Carolina at Chapel Hill (1995)
33. F. Wittmann, O. Lambercy, R. Gassert, Magnetometer-based drift correction during rest in IMU arm motion tracking. *Sensors* **19**, 1312 (2019)
34. A. Carullo, M. Parvis, An ultrasonic sensor for distance measurement in automotive applications. *IEEE Sensors J.* **1**(2), 143 (2001)
35. Acuity, *Principles of Measurement Used by Laser Sensors and Scanners* (Acuity, Toronto, 2016)
36. SICK Sensor Intelligence, *Operating Instructions S300 Safety Laser Scanner* (SICK AG, Waldkirch, 2019)
37. A. Aguirre, S.D. Sierra M., M. Munera, C.A. Cifuentes, Online system for gait parameters estimation using a LRF sensor for assistive devices. *IEEE Sens. J.* 1–1 (2020). <https://doi.org/10.1109/JSEN.2020.3028279>
38. A. Ancillao, S. Tedesco, J. Barton, B. O'Flynn, Indirect measurement of ground reaction forces and moments by means of wearable inertial sensors: a systematic review. *Sensors* **18**(8), 2564 (2018)
39. J. Taborri, E. Palermo, S. Rossi, P. Cappa, Gait partitioning methods: a systematic review. *Sensors* **16**, 66 (2016)
40. A.M. Howell, T. Kobayashi, H.A. Hayes, K.B. Foreman, S.J.M. Bamberg, Kinetic gait analysis using a low-cost insole. *IEEE Trans. Biomed. Eng.* **60**, 3284–3290 (2013)
41. N.C. Bejarano, E. Ambrosini, A. Pedrocchi, G. Ferrigno, M. Monticone, S. Ferrante, A novel adaptive, real-time algorithm to detect gait events from wearable sensors. *IEEE Trans. Neural Syst. Rehabil. Eng.* **23**(3), 413–422 (2014)
42. D.-H. Lim, W.-S. Kim, H.-J. Kim, C.-S. Han, Development of real-time gait phase detection system for a lower extremity exoskeleton robot. *Int. J. Prec. Eng. Manuf.* **18**, 681–687 (2017)
43. M. Islam, E.T. Hsiao-Weckslar, Detection of gait modes using an artificial neural network during walking with a powered ankle-foot orthosis. *J. Biophys.* (Hindawi Publishing Corporation: Online) **2016**, 7984157 (2016)
44. S. Ding, X. Ouyang, Z. Li, H. Yang, Proportion-based fuzzy gait phase detection using the smart insole. *Sensors Actuat. A: Phys.* **284**, 96–102 (2018)
45. X. Jiang, K.H.T. Chu, M. Khoshnam, C. Menon, A wearable gait phase detection system based on force myography techniques. *Sensors* (Basel, Switzerland) **18** (2018)
46. B. Smith, D. Coiro, R. Finson, R. Betz, J. McCarthy, Evaluation of force-sensing resistors for gait event detection to trigger electrical stimulation to improve walking in the child with cerebral palsy. *IEEE Trans. Neural Syst. Rehabil. Eng.* **10**, 22–29 (2002)
47. D. Gouwanda, A.A. Gopalai, A robust real-time gait event detection using wireless gyroscope and its application on normal and altered gaits. *Med. Eng. Phys.* **37**, 219–225 (2015)
48. L. Yu, J. Zheng, Y. Wang, Z. Song, E. Zhan, Adaptive method for real-time gait phase detection based on ground contact forces. *Gait Posture* **41**, 269–275 (2015)
49. W. Kong, M.H. Saad, M.A. Hannan, A. Hussain, Human gait state classification using artificial neural network, in *2014 IEEE Symposium on Computational Intelligence for Multimedia, Signal and Vision Processing (CIMSIVP)*, December 2014 (IEEE, New York, 2014), pp. 1–5
50. J.-Y. Jung, W. Heo, H. Yang, H. Park, A neural network-based gait phase classification method using sensors equipped on lower limb exoskeleton robots. *Sensors* **15**, 27738–27759 (2015)
51. R. Evans, D. Arvind, Detection of gait phases using Orient specks for mobile clinical gait analysis, in *2014 11th International Conference on Wearable and Implantable Body Sensor Networks*, June 2014 (IEEE, New York, 2014), pp. 149–154
52. J. Taborri, E. Scalona, S. Rossi, E. Palermo, F. Patane, P. Cappa, Real-time gait detection based on Hidden Markov Model: is it possible to avoid training procedure?, in *2015 IEEE International Symposium on Medical Measurements and Applications (MeMeA) Proceedings*, May 2015 (IEEE, New York, 2015), pp. 141–145

53. J. Taborri, S. Rossi, E. Palermo, F. Patanè, P. Cappa, A novel HMM distributed classifier for the detection of gait phases by means of a wearable inertial sensor network. *Sensors* **14**, 16212–16234 (2014)
54. A. Mannini, A.M. Sabatini, Gait phase detection and discrimination between walking–jogging activities using hidden Markov models applied to foot motion data from a gyroscope. *Gait Posture* **36**, 657–661 (2012)
55. A. Mannini, A.M. Sabatini, A hidden Markov model-based technique for gait segmentation using a foot-mounted gyroscope, in *2011 Annual International Conference of the IEEE Engineering in Medicine and Biology Society*, August 2011, vol. 2011 (IEEE, New York, 2011), pp. 4369–4373
56. N. Abaid, P. Cappa, E. Palermo, M. Petrarca, M. Porfiri, Gait detection in children with and without hemiplegia using single-axis wearable gyroscopes. *PloS One* **8**(9), e73152 (2013)
57. A. Mannini, V. Genovese, A.M. Sabatin, Online decoding of hidden Markov models for gait event detection using foot-mounted gyroscopes. *IEEE J. Biomed. Health Inf.* **18**, 1122–1130 (2014)
58. J. Taborri, E. Scalona, E. Palermo, S. Rossi, P. Cappa, Validation of inter-subject training for hidden Markov models applied to gait phase detection in children with cerebral palsy. *Sensors* **15**, 24514–24529 (2015)
59. R. Caldas, M. Mundt, W. Potthast, F. Buarque de Lima Neto, B. Markert, A systematic review of gait analysis methods based on inertial sensors and adaptive algorithms. *Gait Posture* **57**, 204–210 (2017)
60. J. Taborri, E. Palermo, S. Rossi, P. Cappa, Gait partitioning methods: a systematic review. *Sensors* **16**, 66 (2016)
61. M. Yuwono, S.W. Su, Y. Guo, B.D. Moulton, H.T. Nguyen, Unsupervised nonparametric method for gait analysis using a waist-worn inertial sensor. *Appl. Soft Comput.* **14**, 72–80 (2014)
62. E. Guenterberg, A. Yang, H. Ghasemzadeh, R. Jafari, R. Bajcsy, S. Sastry, A method for extracting temporal parameters based on hidden Markov models in body sensor networks with inertial sensors. *IEEE Trans. Inf. Technol. Biomed.* **13**, 1019–1030 (2009)
63. P. Catalfamo, S. Ghoussayni, D. Ewins, Gait event detection on level ground and incline walking using a rate gyroscope. *Sensors (Basel, Switzerland)* **10**(6), 5683–702 (2010)
64. A. Sabatini, C. Martelloni, S. Scapellato, F. Cavallo, Assessment of walking features from foot inertial sensing. *IEEE Trans. Biomed. Eng.* **52**, 486–494 (2005)
65. Y. Gurevich, Sequential abstract-state machines capture sequential algorithms. *ACM Trans. Comput. Log.* **1**(1), 77–111 (2000)
66. E. Börger, The abstract state machines method for high-level system design and analysis, in *Formal Methods: State of the Art and New Directions* (Springer, New York, 2010), pp. 79–116
67. D. Kotiadis, H. Hermens, P. Veltink, Inertial gait phase detection for control of a drop foot stimulator. *Med. Eng. Phys.* **32**, 287–297 (2010)
68. M.D. Sánchez Manchola, M.J. Pinto Bernal, M. Munera, C.A. Cifuentes, Gait phase detection for lower-limb exoskeletons using foot motion data from a single inertial measurement unit in hemiparetic individuals. *Sensors* **19**, 2988 (2019)
69. D. Kotiadis, H.J. Hermens, P.H. Veltink, Inertial gait phase detection for control of a drop foot stimulator: inertial sensing for gait phase detection. *Med. Eng. Phys.* **32**(4), 287–297 (2010)
70. N. Limnios, G. Oprisan, *Semi-Markov Processes and Reliability*. (Springer Science & Business Media, Heidelberg, 2012)
71. P. Blunsom, Hidden Markov models. *Lecture Notes* **15**(18–19), 48 (2004)
72. L. Rabiner, A tutorial on hidden Markov models and selected applications in speech recognition. *Proc. IEEE* **77**(2), 257–286 (1989)
73. M.W. Whittle, Clinical gait analysis: a review. *Hum. Movement Sci.* **15**, 369–387 (1996)
74. H. Stolze, J.P. Kuhtz-buschbeck, C. Mondwurf, A. Boczek-funcke, K. Jo, Gait analysis during treadmill and overground locomotion in children and adults. *Electroencephalogr. Clin. Neurophysiol.* **105**, 490–497 (1997)

75. J. Rueterbories, E.G. Spaich, B. Larsen, O.K. Andersen, Methods for gait event detection and analysis in ambulatory systems. *Med. Eng. Phys.* **32**(6), 545–552 (2010)
76. N. Sekiya, H. Nagasaki, H. Ito, F. Taketo, The invariant relationship between step length and step rate during free walking. *J. Hum. Movement Stud.* **30**(6), 241–257 (1996)
77. W.T. Latt, U.-X. Tan, K.C. Veluvolu, C.Y. Shee, W.T. Ang, Real-time estimation and prediction of periodic signals from attenuated and phase-shifted sensed signals, in *2009 IEEE/ASME International Conference on Advanced Intelligent Mechatronics*, July (IEEE, New York, 2009), pp. 1643–1648
78. V. Bonnet, C. Mazzà, J. McCamley, A. Cappozzo, Use of weighted Fourier linear combiner filters to estimate lower trunk 3D orientation from gyroscope sensors data. *J. NeuroEng. Rehabil.* **10**(1), 29 (2013)
79. V. Bonnet, C. Mazzà, J. McCamley, A. Cappozzo, Use of weighted Fourier linear combiner filters to gyroscope sensors data. *J. Neuroeng. Rehabil.* **10**, 29 (2013)
80. G. Data, Real-time estimation of pathological tremor parameters from gyroscope data. *Sensors* **10**, 2129–2149 (2010)
81. A.F. Neto, J.A. Gallego, E. Rocon, J.L. Pons, R. Ceres, Extraction of user's navigation commands from upper body force interaction in walker assisted gait. *BioMed. Eng. OnLine* **1–16**, 37 (2010)
82. Y. Qi, C.B. Soh, E. Gunawan, K.-S. Low, R. Thomas, Assessment of foot trajectory for human gait phase detection using wireless ultrasonic sensor network. *IEEE Trans. Neural Syst. Rehabil. Eng.* **24**, 88–97 (2016)
83. N.-H. Ho, P. Truong, G.-M. Jeong, Step-detection and adaptive step-length estimation for pedestrian dead-reckoning at various walking speeds using a smartphone. *Sensors* **16**, 1423 (2016)